

Three-Dimensional Dynamic Modeling and Motion Analysis for an Active-Tail-Actuated Robotic Fish with Barycentre Regulating Mechanism

Xingwen Zheng¹, Minglei Xiong^{1,2}, Junzheng Zheng¹, Manyi Wang¹, Runyu Tian^{1,3}, and Guangming Xie^{1,4,5}

Abstract—Dynamic modeling has been capturing attention for its fundamentality in precise locomotion analyses and control of underwater robots. However, the existing researches have mainly focused on investigating two-dimensional motion of underwater robots, and little attention has been paid to three-dimensional dynamic modeling, which is just what we focus on. In this article, a three-dimensional dynamic model of an active-tail-actuated robotic fish with a barycentre regulating mechanism is built by combining Newton’s second law for linear motion and Euler’s equation for angular motion. The model parameters are determined by three-dimensional computer-aided design (CAD) software SolidWorks, HyperFlow-based computational fluid dynamics (CFD) simulation, and grey-box model estimation method. Both kinematic experiments with a prototype and numerical simulations are applied to validate the accuracy of the dynamic model mutually. Based on the dynamic model, multiple three-dimensional motions, including rectilinear motion, turning motion, gliding motion, and spiral motion, are analyzed. The experimental and simulation results demonstrate the effectiveness of the proposed model in evaluating the trajectory, attitude, and motion parameters, including the velocity, turning radius, angular velocity, etc., of the robotic fish.

Index Terms—Three-dimensional dynamic modeling, Newton-Euler method, computational fluid dynamics (CFD), grey-box model estimation, robotic fish.

I. INTRODUCTION

IN recent years, underwater robots including varieties of underwater remotely operated vehicles (ROV), autonomous underwater vehicles (AUV), and bio-inspired aquatic systems [1] have been developed and shown great potentials in promoting marine resource exploitation [2], [3], marine economy development [4], [5], and marine ecological environment protection [6], [7]. The research topics of underwater robots cover locomotion control and optimization [8], [9], underwater navigation and localization [10], [11], environment perception and object recognition [12], [13], underwater communication [14],

[15], etc. In particular, mechanism investigation of dynamic performance of underwater robots is fundamental and critical for the above-mentioned researches. Besides, precise dynamic modeling of underwater robots has always been focus and difficulty in underwater robot research.

For dynamic modeling, the typical modeling methods include Lagrangian dynamics method, Newton-Euler method, Lighthill’s elongated-body theory, Schiehlen method, etc. Basing on the Newton-Euler method, Y. Shi’s group has built a dynamic model of an AUV, and then investigated dynamic model-based trajectory tracking control of planar motions of the AUV [16]–[18], without consideration of three-dimensional motions. J. Yu’s group has formulated a robotic fish dynamics using Schiehlen method [19] and Lagrangian dynamics method [20]. It has been demonstrated that the proposed dynamic model is efficient for seeking backward swimming pattern of the robotic fish [20]. They have also proposed a data-driven dynamic modeling method in which the Newton-Euler formulation is applied to analyze the robotic fish dynamics, and parameters in the dynamic model are identified using experimental data of rectilinear motion and turning motion of the robotic fish, also without investigating three-dimensional motions. F. Zhang’s group has established an analytical model for spiral motion of an underwater glider steered by an internal movable mass block, and experiments in the South China Sea have validated the accuracy of the model for achieving desired spiral motion [21]. They have also explored a dynamic model for a blade-driven glider with gliding motion [22]. However, the motion of glider is different from rhythmic motion of the fin-actuated underwater robot. X. Tan’s group has explored dynamic analyses of a tail-actuated robotic fish [23]–[25] and a fish-like glider [26], [27]. For the tail-actuated robotic fish, Lighthill’s large-amplitude elongated-body theory has been combined with rigid-body dynamics and hybrid tail dynamics for building a dynamic model [23]–[25]. However, only surface motion of the robotic fish has been explored. For the fish-like glider, they have built a Newton-Euler method based dynamic model for investigating spiraling maneuver [26] and gliding motion [27]. However, the fish-like glider is just driven by displacing an internal movable mass and pumping fluids, while its tail is not active, without a continuously varied tail angle.

The above-mentioned studies have demonstrated that dynamic modeling is fundamental and essential for locomotion analysis of underwater robots. However, most of the researches have only focused on investigating two-dimensional motions

¹Xingwen Zheng, Minglei Xiong, Junzheng Zheng, Manyi Wang, Runyu Tian, and Guangming Xie are with the State Key Laboratory for Turbulence and Complex Systems, Intelligent Biomimetic Design Lab, College of Engineering, Peking University, Beijing, 100871, China. {zhengxingwen, xiongml, zhengjunzheng, wangmanyi, trytian, xiegm}@pku.edu.cn.
Corresponding author: G. Xie.

²Minglei Xiong is with the Boya Gongdao (Beijing) Robot Technology Co., Ltd., Beijing, 100084, China.

³Runyu Tian is with the China Aerodynamics Research and Development Center, Mianyang, Sichuan, 621000, China.

⁴Peng Cheng Laboratory, Shenzhen, 518055, China.

⁵Guangming Xie is with the Institute of Ocean Research, Peking University, Beijing, 100871, China.

in horizontal plane or vertical plane. Especially for fin-actuated underwater robots, though there are a few preliminary works that have considered dynamic modeling in three-dimensional space [19], [20], [28], the proposed models are typically validated by limited experiments, without validation in a large-scale parameter space. Besides, for three species of underwater robots including active-fin-actuated underwater robot with barycentre regulating mechanism, blade-driven underwater robot [22], and internal movable mass block-driven underwater robot [24], all of which can adjust their centers of mass, there exist significant differences among their dynamics, because an active-fin-actuated underwater robot with barycentre regulating mechanism is able to generate extra rhythmic oscillation of robot body. However, dynamic modelling for such an underwater robot has been rarely investigated.

On the basis of the above analyses, this article mainly focuses on investigating three-dimensional dynamic modeling in a large-scale parameter space for an active-tail-actuated robotic fish with a barycentre regulating mechanism, which has been rarely investigated. Multiple swimming patterns including rectilinear motion, turning motion, gliding motion, and spiral motion are investigated. Firstly, a mathematical description of the dynamic model is proposed basing on Newton-Euler method. Then multiple methods, including SolidWorks software, computational fluid dynamics (CFD) simulation, and grey-box model estimation method, are used for determining model parameters. Finally, numerical simulations and massive kinematic experiments with a robotic fish prototype in a large-scale parameter space are applied to mutually validate the accuracy of the dynamic model in predicting key features, including trajectory, attitude, velocity, etc., of the robotic fish.

The remainder of this article is organized as follows. Section II introduces the bio-inspired robotic fish. Section III establishes a Newton-Euler dynamic model for the robotic fish and determines the model parameters. Section IV presents simulation and experiment results. Section V concludes this article with an outline of future work.

II. THE ROBOTIC FISH

Figure 1 (a) shows the hardware configurations of the robotic fish. Its size (Length×Width×Height) is about 29.1 cm×11.6 cm×13.4 cm. It is composed of a 3D-printed shell, a tail, and three compartments, including a control compartment, an engine compartment, a battery compartment, and a pressure acquisition system compartment. Figure 1 (b) shows the interior of the engine compartment. Three motors, which serve different functions, are wrapped in the engine compartment. Specifically, motor 1 is connected with the tail. It is used to generate propulsive force. Motor 2 is used for driving a rotating bracket. The bracket is connected to motor 3 and a crank-slider mechanism. Motor 3 is used to drive the crank-slider mechanism mentioned above to which a weight block is connected. Through controlling motor 2 and 3, the weight block can move along the direction parallel to principal axis of the robotic fish and rotate about output shaft of motor 2. By controlling the three motors using given frequency, amplitude, and offset parameters, the robotic fish can realize rectilinear

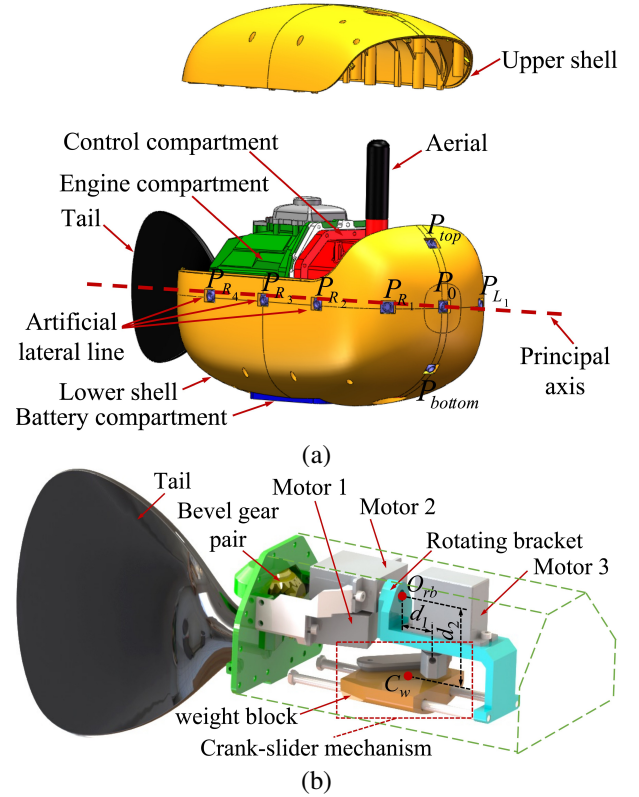


Fig. 1. Hardware configurations of the robotic fish. (a) CAD model of the robotic fish. Eleven pressure sensors named P_{top} , P_{bottom} , P_0 , P_{L_i} , and P_{R_i} ($i = 1, 2, 3, 4$) are mounted on the surface of the shell for establishing an artificial lateral line system (ALLS). ALLS is used to measure the hydrodynamic pressure variations surrounding fish body. More information about the ALLS can be found in our previous work [12]. (b) The diagrammatic sketch of the interior of the engine compartment. d_1 indicates the distance between the output shaft of motor 3 and the connection point O_{rb} of motor 2 and rotating bracket. d_2 indicates the distance between the output shaft of motor 2 and center of mass C_w of the weight block.

motion, turning motion, gliding motion, and spiral motion, as shown in Figure 2. More about motions of the robotic fish can be in the supplementary video.

III. DYNAMIC ANALYSIS FOR THE ROBOTIC FISH

A. Definition of the Coordinate Systems

Figure 3 shows the coordinate systems of the robotic fish. $O_I x_I y_I z_I$, $O_b x_b y_b z_b$, $O_{rb} x_{rb} y_{rb} z_{rb}$, and $O_t x_t y_t z_t$ indicate the global inertial coordinate system, the body-fixed coordinate system, the rotating-bracket-fixed coordinate system, and the tail-fixed coordinate system, respectively. The origin O_b is fixed at the intersection of horizontal section and longitudinal section of the robotic fish, above center of mass C_m of the robotic fish. The longitudinal section is the symmetrical plane of the shell. The horizontal section coincides with the symmetrical plane of the tail and is perpendicular to the longitudinal plane. The origin O_{rb} is fixed at the connection point of motor 2 and the rotating bracket in Figure 1 (c), and expressed as $[a_{rb}, b_{rb}, c_{rb}]$ in $O_b x_b y_b z_b$. The origin O_t is fixed at the connection point of the tail and the engine compartment, and expressed as $[a_t, b_t, c_t]$ in $O_b x_b y_b z_b$. $O_I x_I y_I z_I$ coincides with the initial $O_b x_b y_b z_b$.

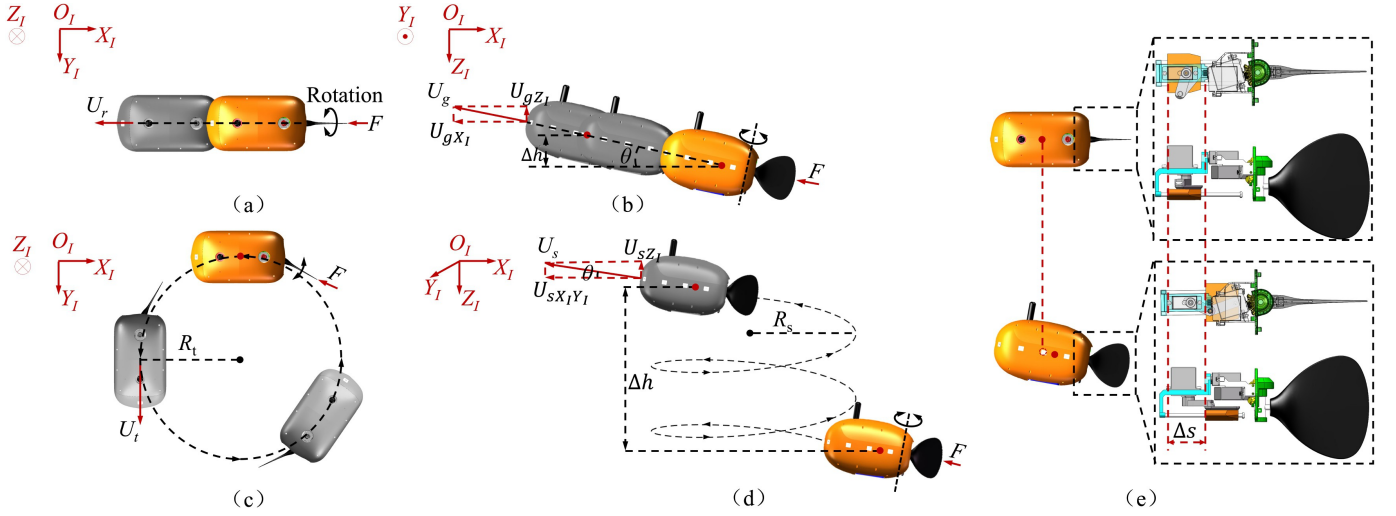


Fig. 2. Multiple three-dimensional swimming patterns of the robotic fish. (a) Rectilinear motion. (b) Gliding motion. (c) Turning motion. (d) Spiral motion. (e) The red point on fish shell means center of mass. It moves backward/forward when the weight block moves backward/forward with a distance of Δs in gliding motion and spiral motion (lower), comparing with rectilinear motion and turning motion (upper). The tails in turning motion and spiral motion have non-zero offsets compared to those in rectilinear motion and gliding motion. U_k ($k = r, t, g, s$) indicates the movement velocity of the robotic fish. U_g is the resultant velocity of the velocity V_{gz_I} along the axis $O_I Z_I$ and the velocity V_{gx_I} along the axis $O_I X_I$. U_s is the resultant velocity of the velocity V_{sz_I} along the axis $O_I Z_I$ and the velocity $V_{sx_I Y_I}$ on $X_I - Y_I$ plane. R_t and R_s indicates the radius in turning motion and spiral motion, respectively. Δh indicates depth variation of the robotic fish. θ indicates pitch angle of the robotic fish.

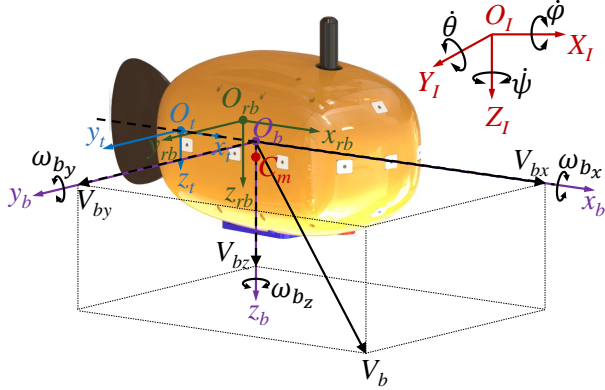


Fig. 3. Definitions of coordinate systems of the robotic fish.

B. Three-Dimensional Kinematic Analysis

1) *Translational Motion of the Robotic Fish:* The position of the robotic fish is denoted as $C_I = [x_I, y_I, z_I]^T$ in $O_I X_I Y_I Z_I$. The velocity of robotic fish is denoted as $V_I = [V_{Ix}, V_{Iy}, V_{Iz}]^T$ in $O_I X_I Y_I Z_I$ and $V_b = [V_{bx}, V_{by}, V_{bz}]^T$ in $O_b x_b y_b z_b$, respectively. The relationship between V_I and V_b is expressed as

$$V_I = \dot{C}_I = R_{bI} \cdot V_b \quad (1)$$

where R_{bI} is the transformation matrix from $O_b x_b y_b z_b$ to $O_I x_I y_I z_I$, taking the form as

$$R_{bI} = \begin{bmatrix} c_\psi c_\theta & -s_\psi c_\theta + c_\psi s_\theta s_\varphi & s_\psi s_\theta + c_\psi s_\theta c_\varphi \\ s_\psi c_\theta & c_\psi c_\theta + s_\psi s_\theta s_\varphi & -c_\psi s_\theta + s_\psi s_\theta c_\varphi \\ -s_\theta & c_\theta s_\varphi & c_\theta c_\varphi \end{bmatrix} \quad (2)$$

where φ , θ , and ψ indicate roll, pitch, and yaw angle of the robotic fish, respectively.

2) *Rotational Motion of the Robotic Fish:* The angular velocity of the robotic fish is denoted as $\omega_b = [\omega_{bx}, \omega_{by}, \omega_{bz}]^T$ in $O_b x_b y_b z_b$ and $\omega_I = [\dot{\varphi}, \dot{\theta}, \dot{\psi}]^T$ in $O_I x_I y_I z_I$. The relationship between ω_b and ω_I is expressed as

$$\omega_I = \begin{bmatrix} 1 & \sin\varphi \tan\theta & \cos\varphi \tan\theta \\ 0 & \cos\varphi & -\sin\varphi \\ 0 & \sin\varphi / \cos\theta & \cos\varphi / \cos\theta \end{bmatrix} \cdot \omega_b \quad (3)$$

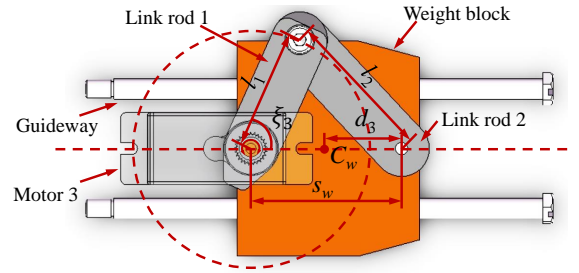


Fig. 4. Crank-slider mechanism with the weight block. l_1 and l_2 indicate the lengths of the link rods. d_3 indicates the distance between center of mass of the weight block C_w and connecting point of the weight block and link rod 2. s_w indicates the distance between output shaft of motor 3 and connecting point of the weight block and link rod 2. The masses of guideway, motor 3, link rod 1, and link 2 are all ignored.

3) *Motion analysis of the weight block:* As shown in Figure 1 (c), the weight block is able to rotate through controlling output angle ξ_2 of motor 2. Thus roll angle φ of the robotic fish is able to be adjusted. On the other hand, as shown in Figure 4, the distance s_w is able to be adjusted through controlling output angle ξ_3 of motor 3. Thus the weight block

is able to move along the guideway, and pitch angle θ of the robotic fish is able to be adjusted. s_w takes the form as

$$s_w = s_{w_0} + \Delta d \quad (4)$$

where s_{w_0} indicates the initial value of s_w , with which pitch angle and roll angle of the robotic fish are 0. Δd is the distance between the weight block's current position and its initial position in the kinematics experiments.

The coordinate of center of mass of the weight block $C_w[x_{C_w}, y_{C_w}, z_{C_w}]$ is expressed in $O_b x_b y_b z_b$, taking the form as

$$\begin{aligned} x_{C_w} &= a_{rb} + d_1 - (s_w - d_3) \\ y_{C_w} &= b_{rb} + d_2 \cdot \sin \xi_2 \\ z_{C_w} &= c_{rb} + d_2 \cdot \cos \xi_2 \end{aligned} \quad (5)$$

The coordinate of center of mass of the robotic fish $C_m[x_{C_m}, y_{C_m}, z_{C_m}]$ takes the form as

$$j_{C_m} = \frac{(M_{ew_j} + M_{w_j})}{m_{total}} \quad (6)$$

where $j = x, y, z$, M_{ew_j} is static moment about the $O_b j_b$ axis for the part apart from the weight block. M_{w_j} is static moment about the $O_b j_b$ axis for the weight block, taking the form as

$$M_{w_j} = m_w \cdot j_{C_w} \quad (7)$$

where m_w is the mass of the weight block.

The initial coordinate of center of mass of the robotic fish is expressed as $[x_{C_{m0}}, y_{C_{m0}}, z_{C_{m0}}]$. Besides, both pitch angle θ and roll angle φ of the robotic fish are zero when the weight block is at its initial position.

C. Three-Dimensional Force Analysis

In this part, the forces and torques acting on the tail and fish body of the robotic fish are analyzed. For the tail, the lift and drag are considered. For the fish body, we respectively consider lift force and drag force in $x_b - z_b$ plane and $x_b - y_b$ plane, gravity, buoyancy, and impact of water flow.

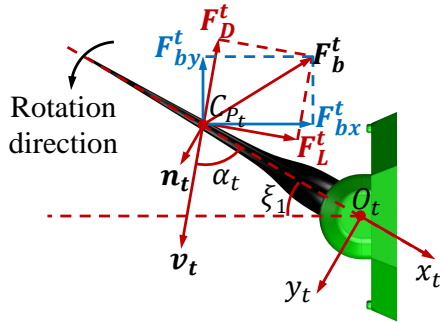


Fig. 5. Force analysis for the tail. C_{pt} is center of press of the tail, and it is coincident with center of mass of the tail.

1) *Force Analysis for the Tail:* For the tail of the robotic fish, its time-varying oscillating angle ξ_1 is expressed as

$$\xi_1(t) = \bar{\xi}_1 + A_1 \sin(2\pi f_1 t) \quad (8)$$

where $\bar{\xi}_1$, A_1 , and f_1 are the oscillating offset, amplitude, and frequency of the tail, respectively.

The velocity of C_{pt} in Figure 5 is expressed as

$$\mathbf{v}_t = \mathbf{V}_b + \boldsymbol{\omega}_b \times \mathbf{O}_b C_{pt} + \boldsymbol{\omega}_t \times \mathbf{O}_t C_{pt} \quad (9)$$

where $\mathbf{O}_b C_{pt}$ is the vector from O_b to C_{pt} . It is expressed as

$$\mathbf{O}_b C_{pt} = (a_t - r_c \cdot \cos \xi_1) \cdot \hat{\mathbf{x}}_b + (b_t - r_c \cdot \sin \xi_1) \cdot \hat{\mathbf{y}}_b + c_t \cdot \hat{\mathbf{z}}_b \quad (10)$$

where $\hat{\mathbf{x}}_b$, $\hat{\mathbf{y}}_b$, and $\hat{\mathbf{z}}_b$ are unit vector along the $O_b x_b$ axis, $O_b y_b$ axis, and $O_b z_b$ axis in $O_b x_b y_b z_b$, respectively. $\mathbf{O}_t C_{pt}$ is the vector from O_t to C_{pt} , and it is expressed as

$$\mathbf{O}_t C_{pt} = -r_c \cdot \cos \xi_1 \cdot \hat{\mathbf{x}}_b - r_c \cdot \sin \xi_1 \cdot \hat{\mathbf{y}}_b + 0 \cdot \hat{\mathbf{z}}_b \quad (11)$$

$\boldsymbol{\omega}_t$ is the oscillating angular velocity of the tail, and it is expressed as

$$\boldsymbol{\omega}_t = \dot{\xi}_1 \cdot \hat{\mathbf{z}}_b = 2\pi f_1 A_1 \cos(2\pi f_1 t) \cdot \hat{\mathbf{z}}_b \quad (12)$$

The tail of the robotic fish is regarded as a rigid plate without spanwise wave motion, which is different from fins in [29]. There are various forms of tail-generated force and torque [25], [28], [30]–[33] for different of types of tails. Here, we have adopted forms as in [25], [28], [33], which are typically applied to express torque and force caused by a rigid plate-like tail. Specifically, the lift F_L^t and drag F_D^t of the tail are expressed as

$$F_\lambda^t = \frac{1}{2} \rho |\mathbf{v}_t|^2 S_t C_{\lambda_t}(|\alpha_t|) \quad (13)$$

where $\lambda = L, D$. ρ is the density of water. S_t is the surface area of the tail. C_{L_t} and C_{D_t} are force coefficients which will be determined in section III. E. α_t is the angle of attack of the tail, which is expressed as

$$\alpha_t = \arcsin(\mathbf{n}_t \cdot \hat{\mathbf{v}}_t) \quad (14)$$

where \mathbf{n}_t is the normal vector of the tail, which is expressed as

$$\mathbf{n}_t = -\sin \xi_1 \cdot \hat{\mathbf{x}}_b + \cos \xi_1 \cdot \hat{\mathbf{y}}_b + 0 \cdot \hat{\mathbf{z}}_b \quad (15)$$

Basing on the above analyses, the three-dimensional drag F_D^t [34] acting on the tail is expressed as

$$\mathbf{F}_D^t = -F_D^t \hat{\mathbf{v}}_t \quad (16)$$

The three-dimensional lift F_L^t acting on the tail is expressed as

$$\mathbf{F}_L^t = \begin{cases} \frac{\mathbf{v}_t \sin \alpha_t - \mathbf{n}_t}{\|\mathbf{v}_t \sin \alpha_t - \mathbf{n}_t\|} \cdot F_L^t & \text{if } \mathbf{n}_t \cdot \hat{\mathbf{v}}_t > 0 \\ \frac{\mathbf{v}_t \sin \alpha_t + \mathbf{n}_t}{\|\mathbf{v}_t \sin \alpha_t + \mathbf{n}_t\|} \cdot F_L^t & \text{if } \mathbf{n}_t \cdot \hat{\mathbf{v}}_t \leq 0 \end{cases} \quad (17)$$

Then, the tail-generated torque M_b^t acting on the robotic fish is expressed as

$$\mathbf{M}_b^t = \mathbf{O}_b C_{pt} \times (\mathbf{F}_L^t + \mathbf{F}_D^t) \quad (18)$$

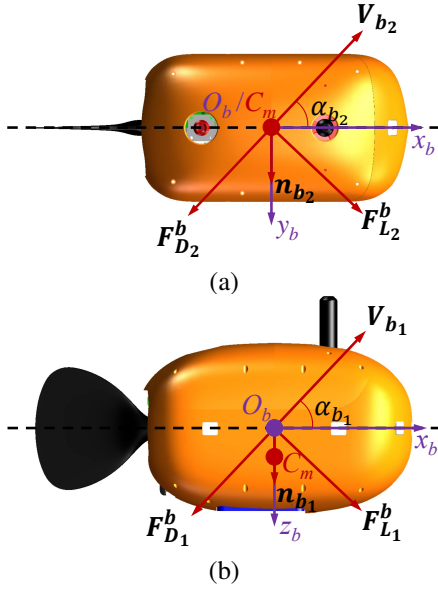


Fig. 6. Force analysis for the fish body. (a) Force analysis for $x_b - z_b$ plane. (b) Force analysis for $x_b - y_b$ plane.

2) *Force Analysis for Fish Body*: Figure 6 shows the drag $F_{D_i}^b$ ($i = 1, 2$) and lift $F_{L_i}^b$ ($i = 1, 2$) acting on the fish body, of which the values are expressed as

$$\begin{aligned} F_{D_i}^b &= \frac{1}{2} \rho |\mathbf{V}_{b_i}|^2 S_{b_i} C_{D_{b_i}}(|\alpha_{b_i}|) \\ F_{L_i}^b &= \frac{1}{2} \rho |\mathbf{V}_{b_i}|^2 S_{b_i} C_{L_{b_i}}(|\alpha_{b_i}|) \end{aligned} \quad (19)$$

where $C_{D_{b_i}}$ and $C_{L_{b_i}}$ are force coefficients which will be determined in section III. E.

$$\begin{aligned} \mathbf{V}_{b_1} &= V_{bx} \cdot \hat{\mathbf{x}}_b + V_{bz} \cdot \hat{\mathbf{z}}_b \\ \mathbf{V}_{b_2} &= V_{bx} \cdot \hat{\mathbf{x}}_b + V_{by} \cdot \hat{\mathbf{y}}_b \end{aligned} \quad (20)$$

S_{b_i} ($i = 1, 2$) is the surface area tensor of the robotic fish. It is defined as

$$S_{b_i} = \hat{\mathbf{V}}_{b_i}^T \cdot \mathbf{A}_i \cdot \hat{\mathbf{V}}_{b_i}, (i = 1, 2) \quad (21)$$

where

$$\mathbf{A}_1 = \begin{bmatrix} S_{xx} & S_{xz} \\ S_{zx} & S_{zz} \end{bmatrix}, \mathbf{A}_2 = \begin{bmatrix} S_{xx} & S_{xy} \\ S_{yx} & S_{yy} \end{bmatrix} \quad (22)$$

\mathbf{A}_1 and \mathbf{A}_2 are diagonal matrices. S_{xx} , S_{yy} , and S_{zz} indicates the maximum cross section area perpendicular to the axes $O_b x_b$, $O_b y_b$, and $O_b z_b$. α_{b_i} ($i = 1, 2$) is angle of attack of fish body, taking the form as

$$\alpha_{b_i} = \arcsin(\mathbf{n}_{b_i} \cdot \hat{\mathbf{V}}_{b_i}) \quad (23)$$

\mathbf{n}_{b_i} ($i = 1, 2$) is the normal vector, taking the form as

$$\mathbf{n}_{b_1} = \hat{\mathbf{z}}_b, \mathbf{n}_{b_2} = \hat{\mathbf{y}}_b \quad (24)$$

Basing on the above-analyses, the three-dimensional drag $F_{D_i}^b$ ($i = 1, 2$) is expressed as

$$\mathbf{F}_{D_i}^b = -F_{D_i}^b \hat{\mathbf{V}}_{b_i} \quad (25)$$

The three-dimensional lift $F_{L_i}^b$ ($i = 1, 2$) is expressed as

$$\mathbf{F}_{L_i}^b = \begin{cases} \frac{V_{b_i} \sin \alpha_{b_i} - \mathbf{n}_{b_i}}{\|\mathbf{V}_{b_i} \sin \alpha_{b_i} - \mathbf{n}_{b_i}\|} \cdot F_{L_i}^b & \text{if } \mathbf{n}_{b_i} \cdot \hat{\mathbf{V}}_{b_i} > 0 \\ \frac{V_{b_i} \sin \alpha_{b_i} + \mathbf{n}_{b_i}}{\|\mathbf{V}_{b_i} \sin \alpha_{b_i} + \mathbf{n}_{b_i}\|} \cdot F_{L_i}^b & \text{if } \mathbf{n}_{b_i} \cdot \hat{\mathbf{V}}_{b_i} \leq 0 \end{cases} \quad (26)$$

Besides, rotations of the robotic fish cause damping torques M_ω acting on fish body, and M_ω is expressed as

$$\mathbf{M}_\omega = C_{\omega_b} \cdot \boldsymbol{\omega}_b \quad (27)$$

where C_{ω_b} is damping torque coefficient, taking the form as

$$C_{\omega_b} = \text{diag}\{C_{\omega_{b_1}}, C_{\omega_{b_2}}, C_{\omega_{b_3}}\} \quad (28)$$

In addition, the robotic fish is subjected to torque M_I caused by impact of water flow, and M_I [34] is expressed as

$$\mathbf{M}_I = M_{I_{x_b}} \cdot \hat{\mathbf{x}}_b + M_{I_{y_b}} \cdot \hat{\mathbf{y}}_b + M_{I_{z_b}} \cdot \hat{\mathbf{z}}_b \quad (29)$$

where

$$\begin{aligned} M_{I_{x_b}} &= 0 \\ M_{I_{y_b}} &= \frac{1}{2} \rho |\mathbf{V}_{b_1}|^2 S_{b_1} C_{M_{I_{y_b}}}(\alpha_{b_1}) \\ M_{I_{z_b}} &= \frac{1}{2} \rho |\mathbf{V}_{b_2}|^2 S_{b_2} C_{M_{I_{z_b}}}(\alpha_{b_2}) \end{aligned} \quad (30)$$

$C_{M_{I_{y_b}}}$ and $C_{M_{I_{z_b}}}$ are torque coefficients which will be determined in section III. E.

3) *The Effect of Gravity and Buoyance*: The gravity \mathbf{F}_g and buoyancy \mathbf{F}_b of the robotic fish are expressed in $O_b x_b y_b z_b$, taking the form as

$$\mathbf{F}_g = m_{total} \cdot \mathbf{R}_{bI}^{-1} \cdot \mathbf{g} \quad (31)$$

$$\mathbf{F}_b = -m_b \cdot \mathbf{R}_{bI}^{-1} \cdot \mathbf{g} \quad (32)$$

where m_{total} and m_b are total mass and buoyancy mass of the robotic fish, respectively.

The torque \mathbf{M}_g caused by the buoyance of the robotic fish is expressed as

$$\mathbf{M}_g = \mathbf{O}_b \mathbf{C}_m \times \mathbf{F}_g \quad (33)$$

where $\mathbf{O}_b \mathbf{C}_m$ is the vector from O_b to C_m , taking the form as

$$\mathbf{O}_b \mathbf{C}_m = x_{C_m} \hat{\mathbf{x}}_b + y_{C_m} \hat{\mathbf{y}}_b + z_{C_m} \hat{\mathbf{z}}_b \quad (34)$$

D. Newton-Euler Dynamic Model

Basing on Newton's second law, the total force \mathbf{F}_{total} acting on the robotic fish is expressed as

$$\begin{cases} \mathbf{F}_{total} = \mathbf{F}_g + \mathbf{F}_b + \mathbf{F}_{L_1}^b + \mathbf{F}_{D_1}^b + \mathbf{F}_{L_2}^b + \mathbf{F}_{D_2}^b + \mathbf{F}_L^t + \mathbf{F}_D^t \\ \mathbf{F}_{total} = \frac{dM\mathbf{V}_{C_m}}{dt} \end{cases} \quad (35)$$

where $M = \text{diag}\{m_{total}, m_{total}, m_{total}\}$. \mathbf{V}_{C_m} indicates velocity of center of mass C_m of the robotic fish, taking the form as

$$\mathbf{V}_{C_m} = \mathbf{V}_b + \boldsymbol{\omega}_b \times \mathbf{O}_b \mathbf{C}_m \quad (36)$$

$$\frac{d\mathbf{V}_{C_m}}{dt} = \frac{d\mathbf{V}_b}{dt} + \frac{d\boldsymbol{\omega}_b}{dt} \times \mathbf{O}_b \mathbf{C}_m + \boldsymbol{\omega}_b \times \mathbf{V}_b + \boldsymbol{\omega}_b \times (\boldsymbol{\omega}_b \times \mathbf{O}_b \mathbf{C}_m)$$

Basing on Euler's equation, the total torque M_{total} about C_m is expressed as

$$\begin{cases} M_{total} = \frac{dH_{C_m}}{dt} \\ M_{total} = M_g + M_\omega + M_b^t + M_I - O_b C_m \times F_{total} \end{cases} \quad (38)$$

where H_{C_m} is the moment of momentum about C_m of the robotic fish, taking the form as

$$H_{C_m} = J\omega_b + M \cdot O_b C_m \times V_b \quad (39)$$

$$\begin{aligned} \frac{dH_{C_m}}{dt} = & J\dot{\omega}_b + \omega_b \times (J\omega_b) + M \cdot (\omega_b \times O_b C_m) \times V_b \\ & + M \cdot O_b C_m \times (\dot{V}_b + \omega_b \times V_b) \end{aligned} \quad (40)$$

$J = \text{diag}\{J_{xx}, J_{yy}, J_{zz}\}$ is the moment of inertia about O_b for the robotic fish, taking the form as

$$J = J_{ew} + J_w \quad (41)$$

J_w and J_{ew} are the moments of inertia about O_b for the weight block and the part apart from weight block, respectively, taking the form as

$$J_\gamma = J_\gamma' + m_\gamma * \text{diag}\{r_{O_b C_\gamma x}^2, r_{O_b C_\gamma y}^2, r_{O_b C_\gamma z}^2\} \quad (42)$$

where $\gamma = ew, w$. 'ew' and 'w' indicate the part apart from the weight block and the weight block, respectively. m_{ew} is mass of the part apart from the weight block, and $m_{ew} = m_{total} - m_w$. $r_{O_b C_\gamma x}$, $r_{O_b C_\gamma y}$, and $r_{O_b C_\gamma z}$ are components of the distance between C_m and C_γ along the $O_b x_b$ axis, $O_b y_b$ axis, and $O_b z_b$ axis, respectively, taking the form as

$$\begin{aligned} r_{O_b C_\gamma x}^2 &= y_{C_\gamma}^2 + z_{C_\gamma}^2 \\ r_{O_b C_\gamma y}^2 &= x_{C_\gamma}^2 + z_{C_\gamma}^2 \\ r_{O_b C_\gamma z}^2 &= x_{C_\gamma}^2 + y_{C_\gamma}^2 \end{aligned} \quad (43)$$

where $[x_{C_{ew}}, y_{C_{ew}}, z_{C_{ew}}]$ is coordinate of center of mass for the part apart from the weight block. $j_{C_{ew}} (j = x, y, z)$ takes the form as

$$j_{C_{ew}} = M_{ewj} / m_{ew} \quad (44)$$

J_γ' is the moment of inertia about C_γ for the part apart from weight block, taking the form as

$$J_\gamma' = \text{diag}\{J'_{\gamma xx}, J'_{\gamma yy}, J'_{\gamma zz}\} \quad (45)$$

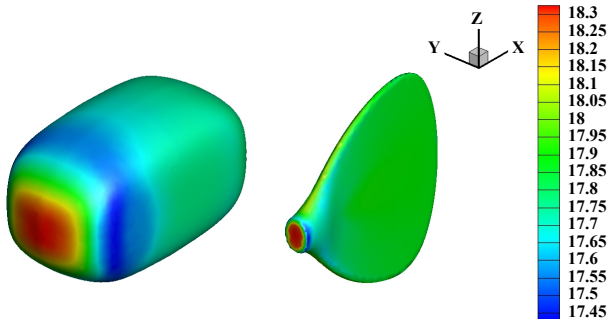


Fig. 7. Hydrodynamic pressure variations on the surface of the fish body and tail when α_{b_1} , α_{b_2} , and α_t are 0.

Basing on the above analyses, the concrete form of the dynamic equations (35) and (38) can be finally acquired, as shown in (46) where F_{x_b} , F_{y_b} , F_{z_b} are components of the total force along the $O_b x_b$ axis, $O_b y_b$ axis, and $O_b z_b$ axis, respectively. M_{x_b} , M_{y_b} , M_{z_b} are components of the total torque about the $O_b x_b$ axis, $O_b y_b$ axis, and $O_b z_b$ axis, respectively.

E. Determination of Model Parameters

In this part, model parameters, which include mass, dimensions, and moment of inertia of the robotic fish, etc. are determined by three-dimensional computer-aided design (CAD) software SolidWorks, as shown in Table S1 of the supplementary materials. We have used two robotic fish to conduct the experiments. m_{b_1} is buoyancy mass for the robotic fish used in rectilinear motion and turning motion, while m_{b_2} is for the robotic fish used in gliding motion and spiral motion. m_{b_1} and m_{b_2} are both determined by actual measurement. Lift coefficients, drag coefficients, and impact torque coefficients are determined by computational fluid dynamics (CFD) simulation. Damping torque coefficients are determined by grey-box model estimation method.

1) *Determining Force Coefficients and Torque Coefficients Using Computational Fluid Dynamics (CFD) Method:* Specifically, computational fluid dynamics (CFD) simulation for fish body and tail of the robotic fish were respectively conducted using a CFD software called HyperFlow, which is developed by China Aerodynamics Research and Development Center (CARDRC). HyperFlow is a structured/unstructured hybrid integrated fluid simulation software. It is able to run the structured solver synchronously on structured grids and unstructured solver on unstructured grids. Besides, it has been proved to have good performance in multi-purpose fluid simulation [35], [36]. Figure 7 shows the hydrodynamic pressure variations of the tail and fish body using CFD simulation. More details about the CFD simulation can be found in Section S1 of the supplementary materials. In the CFD simulation, angles of attack α_t , α_{b_1} , and α_{b_2} changed from 0 to $\pi/6$ rad with an interval of $\pi/60$ rad. Basing on the hydrodynamic pressure variations, the lift, drag, and impact torque coefficients under certain values of α_t , α_{b_1} , and α_{b_2} are acquired, as shown in Figure 8. Basing on data fitting method, the quantitative equations which link $\alpha_t/\alpha_{b_1}/\alpha_{b_2}$ to coefficients mentioned above can be acquired, as shown in Section S1 of the supplementary materials.

2) *Determining the damping torque coefficients using grey-box model estimation method:* The damping torque coefficients are determined by grey-box model estimation method [37]. In the grey-box model estimation, we recorded the rectilinear velocity of the robotic fish with given oscillating parameters, including amplitude and frequency of the tail in 28 s. The input data for grey-box model were the oscillating parameters, while the output data were the rectilinear velocity. As shown in Table S2 of the supplementary materials, we restricted ranges of the three coefficients for avoiding drift of the solution. The final values of the damping coefficients are shown in Table S2 of the supplementary materials. Figure 9

$$\begin{cases}
F_{x_b} = m_{total} \cdot \left[\dot{V}_{b_x} - V_{b_y} \cdot \omega_{b_z} + V_{b_z} \cdot \omega_{b_y} - x_{C_m} (\omega_{b_z}^2 + \omega_{b_y}^2) + y_{C_m} (\omega_{b_x} \omega_{b_y} - \dot{\omega}_{b_z}) + z_{C_m} (\omega_{b_x} \omega_{b_z} + \dot{\omega}_{b_y}) \right] \\
F_{y_b} = m_{total} \cdot \left[\dot{V}_{b_y} - V_{b_z} \cdot \omega_{b_x} + V_{b_x} \cdot \omega_{b_z} - y_{C_m} (\omega_{b_x}^2 + \omega_{b_z}^2) + z_{C_m} (\omega_{b_y} \omega_{b_z} - \dot{\omega}_{b_x}) + x_{C_m} (\omega_{b_x} \omega_{b_y} + \dot{\omega}_{b_z}) \right] \\
F_{z_b} = m_{total} \cdot \left[\dot{V}_{b_z} - V_{b_x} \cdot \omega_{b_y} + V_{b_y} \cdot \omega_{b_x} - z_{C_m} (\omega_{b_y}^2 + \omega_{b_x}^2) + x_{C_m} (\omega_{b_z} \omega_{b_x} - \dot{\omega}_{b_y}) + y_{C_m} (\omega_{b_y} \omega_{b_z} + \dot{\omega}_{b_x}) \right] \\
M_{x_b} = J_{xx} \dot{\omega}_{b_x} + (J_{zz} - J_{yy}) \omega_{b_y} \omega_{b_z} + m_{total} \cdot \left[y_{C_m} (\dot{V}_{b_z} + V_{b_y} \omega_{b_x} - V_{b_x} \omega_{b_y}) - z_{C_m} (\dot{V}_{b_y} + V_{b_x} \omega_{b_z} - V_{b_z} \omega_{b_x}) \right] \\
M_{y_b} = J_{yy} \dot{\omega}_{b_y} + (J_{xx} - J_{zz}) \omega_{b_z} \omega_{b_x} + m_{total} \cdot \left[z_{C_m} (\dot{V}_{b_x} + V_{b_z} \omega_{b_y} - V_{b_y} \omega_{b_z}) - x_{C_m} (\dot{V}_{b_z} + V_{b_y} \omega_{b_x} - V_{b_x} \omega_{b_y}) \right] \\
M_{z_b} = J_{zz} \dot{\omega}_{b_z} + (J_{yy} - J_{xx}) \omega_{b_x} \omega_{b_y} + m_{total} \cdot \left[x_{C_m} (\dot{V}_{b_y} + V_{b_x} \omega_{b_z} - V_{b_z} \omega_{b_x}) - y_{C_m} (\dot{V}_{b_x} + V_{b_z} \omega_{b_y} - V_{b_y} \omega_{b_z}) \right]
\end{cases} \quad (46)$$

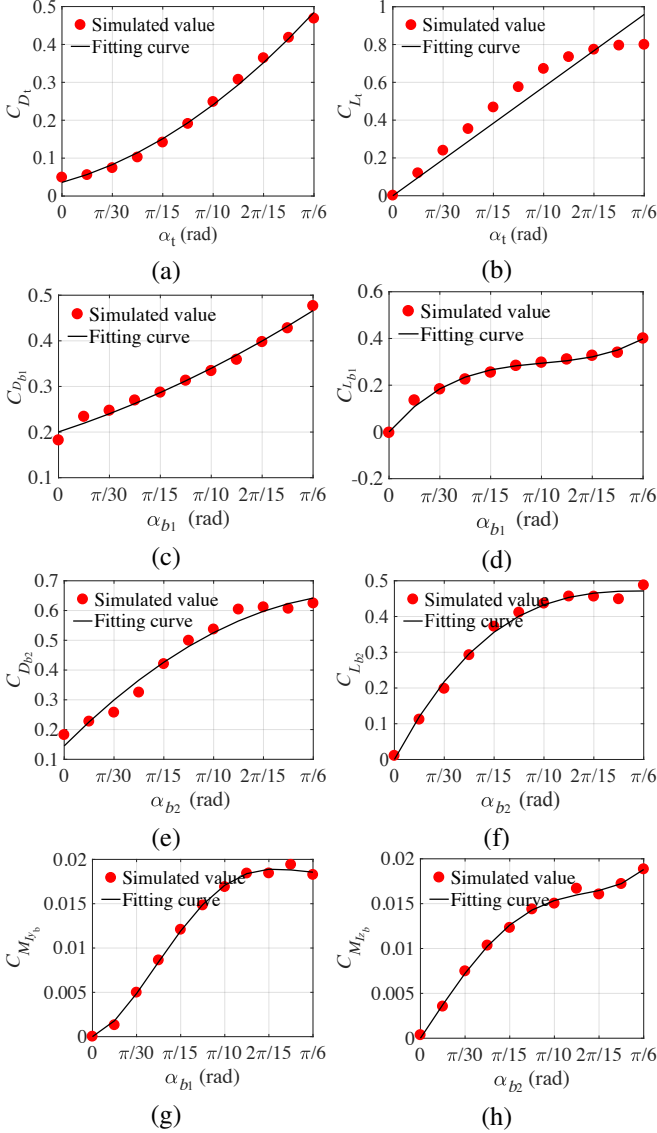


Fig. 8. The lift, drag, and impact torque coefficients acquired by computational fluid dynamics (CFD) simulation. (a) C_{D_t} . (b) C_{L_t} . (c) $C_{D_{b_1}}$. (d) $C_{L_{b_1}}$. (e) $C_{D_{b_2}}$. (f) $C_{L_{b_2}}$. (g) $C_{M_{I_{y_b}}}$. (h) $C_{M_{I_{y_b}}}$.

shows the measured velocity and simulated velocity obtained using the estimated coefficients. The measured velocity and simulated velocity of the robotic fish match with a 61.45% fit.

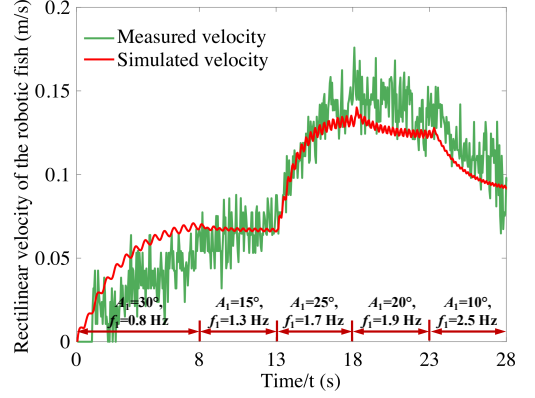


Fig. 9. Measured rectilinear velocity and estimated rectilinear velocity obtained using grey-box model estimation method.

IV. SIMULATIONS AND EXPERIMENTS

A. Rectilinear motion

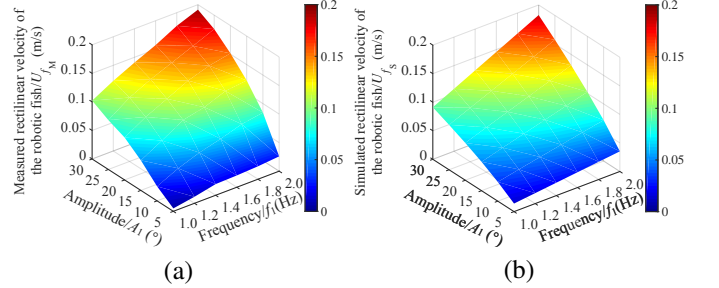


Fig. 10. Measured and simulated rectilinear motion velocity of the robotic fish. (a) Measured value. (b) Simulated value.

In rectilinear motion experiment, varieties of rectilinear velocities were obtained by changing the oscillating frequency f_1 and amplitude A_1 of the tail, while the oscillating offset ξ_1 was zero. Figure 10 shows the measured and simulated rectilinear motion velocity U_r obtained by various combinations of f_1 and A_1 . U_r is the resultant velocity of the velocity V_{I_x} along the axis $O_I X_I$ and the velocity V_{I_y} along the axis $O_I Y_I$. It increases with f_1 and A_1 . The measured and simulated U_r match well with a coefficient of determination (R^2) of 0.8898 and a mean absolute error (MAE) of 0.0137 m/s. Figure 11 shows the real-time attitude of the robotic fish when it was actuated by five combinations of A_1 and f_1 . Under each combination of A_1 and f_1 , yaw angle of the robotic fish oscillates around a certain value while roll and pitch angle of the robotic fish oscillate around zero, in which case the

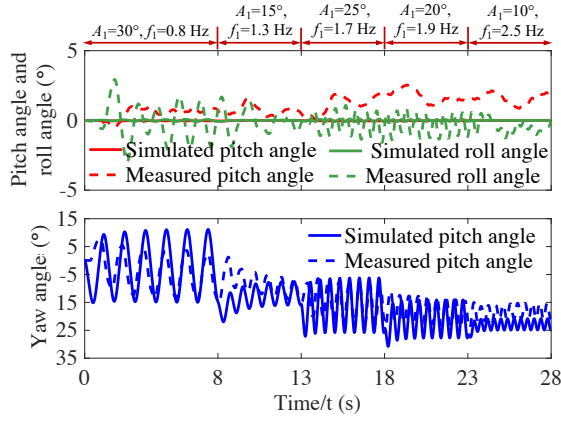


Fig. 11. Real-time attitudes of the robotic fish in rectilinear motion.

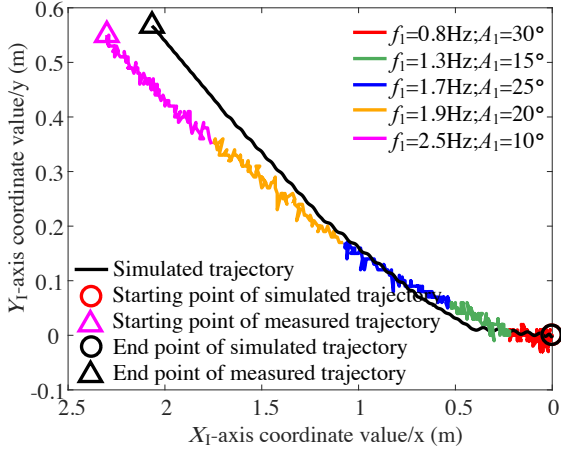


Fig. 12. Trajectory of the robotic fish under five combinations of A_1 and f_1 .

robotic fish swims in a straight line. Because of the periodical oscillation of the tail, the robotic fish body oscillates while swimming. Thus the yaw angle, pitch angle, and roll angle of the robotic fish oscillate periodically with the time. It can be seen that the simulated and measured attitudes match well in the oscillatory feature and value. A more careful inspection revealed that the yaw amplitude increases with the increasing A_1 while the yaw rate increases with the increasing f_1 . For pitch angle and roll angle, the biggest errors between the estimated values and the measured values are both less than 3° , which are small enough. The errors are results of the wave motion of water which caused the roll motion and pitch motion of the robotic fish. The final trajectory of the robotic fish is shown in Figure 12, with a maximum error between the simulated trajectory and measured trajectory of 0.2407 m.

B. Turning motion

In turning motion experiment, varieties of turning angular velocities ω_t and turning radii R_t were obtained by various combinations of oscillating offset $\bar{\xi}_1$ and frequency f_1 of the tail. As shown in Figure 13 and Figure 14, the measured value and simulated value of ω_t match well with $R^2=0.7462$ and $MAE=0.0409$ rad/s, while the measured R_t matches the simulated R_t with a $MAE=0.0657$ m and an average

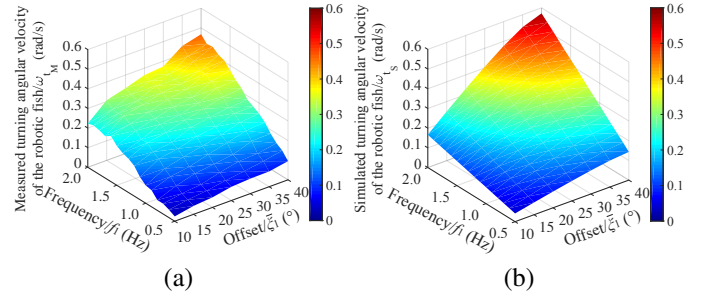


Fig. 13. Measured and simulated turning angular velocity of the robotic fish. (a) Measured value. (b) Simulated value.

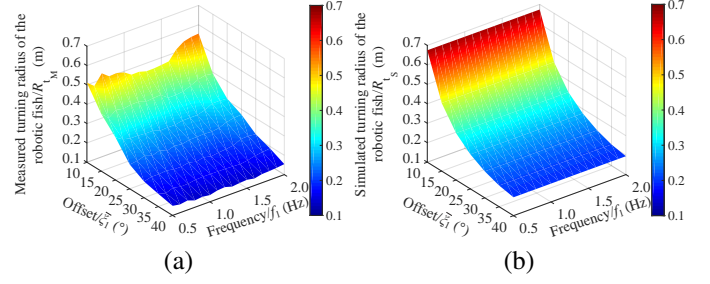


Fig. 14. Measured and simulated turning radius of the robotic fish. (a) Measured value. (b) Simulated value.

percentage error of 18.5913%. The ω_t increases with the increasing $\bar{\xi}_1$ and f_1 . The R_t decreases with the increasing $\bar{\xi}_1$ and it is nearly constant with the f_1 . Figure 15 shows the real-time yaw/pitch/roll rate of the robotic fish. It can be seen that both the roll rate ω_{I_y} and pitch rate ω_{I_x} of the robotic fish oscillate around zero. The yaw rate ω_{I_z} oscillates around a positive value when the value of $\bar{\xi}_1$ is negative, in which case the robotic fish turns left. While the ω_{I_z} oscillates around a negative value when the value of $\bar{\xi}_1$ is positive, in which case the robotic fish turns right. A more careful inspection reveals that the amplitude of the ω_{I_z} increases with the $\bar{\xi}_1$ while decreases with the f_1 , while the rate of ω_{I_z} increases with the f_1 . For the amplitudes of ω_{I_x} and ω_{I_y} , they decrease with the f_1 .

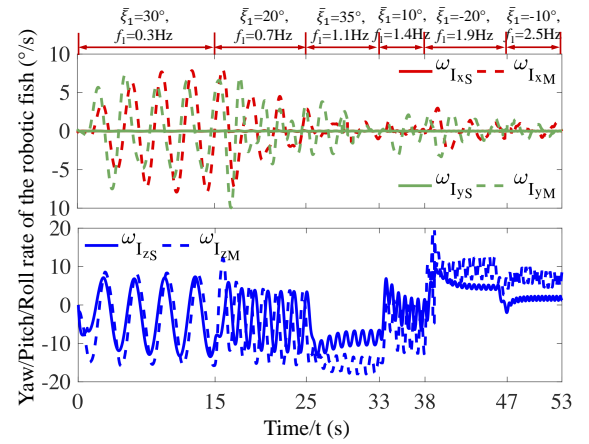


Fig. 15. Real-time yaw/pitch/roll rate of the robotic fish in turning motion under six combinations of $\bar{\xi}_1$ and f_1 . ω_{I_jS} and ω_{I_jM} ($j = x, y, z$) indicate simulated and measured value of the yaw/pitch/roll rate, respectively.

C. Gliding motion

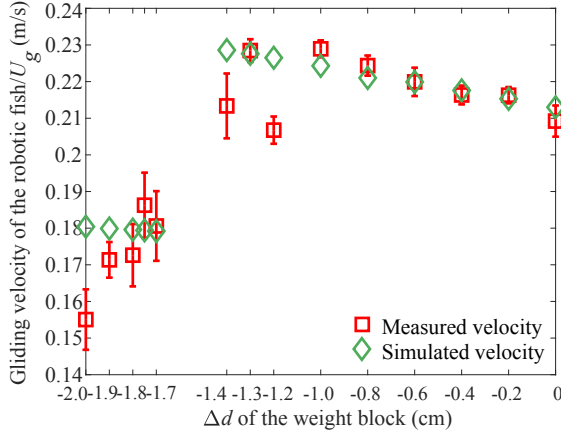


Fig. 16. Measured and simulated gliding velocity of the robotic fish.

In gliding motion experiment, varieties of gliding velocities U_g were obtained by changing Δd of the weight block. A_1 , f_1 , and ξ_1 of the tail are 20° , 2.0 Hz, and 0, respectively. Figure 16 shows the measured and simulated U_g of the robotic fish. The maximum and average percentage errors between the measured and simulated U_g are 14.0507% and 3.5340%, respectively. It is noteworthy that because of the depth limitation of the water tank (only 0.8 m), the robotic fish reached the surface of the water before it reached the state of uniform motion. So the U_g of the robotic fish for $\Delta d = -2.0$ cm, -1.9 cm, -1.8 cm, and -1.7 cm is average gliding velocity of the robotic fish in its acceleration process. While the U_g for Δd varied from -1.4 cm to 0 are velocities when the robotic fish was in uniform motion state. Comparing the U_g for Δd from -1.4 cm to 0, it can be seen that U_g of the robotic fish decreases with the increasing $|\Delta d|$.

D. Spiral motion

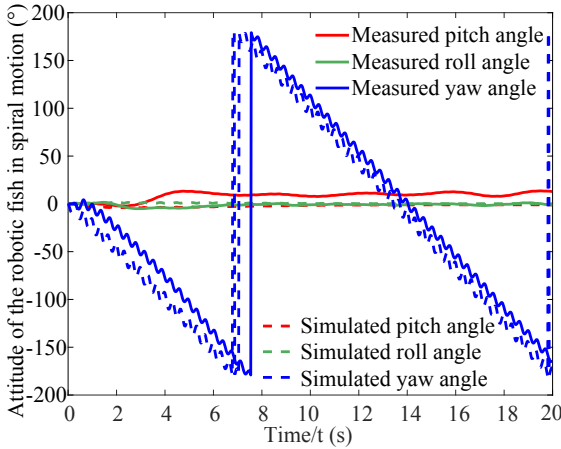


Fig. 17. Real-time measured and simulated attitude of the robotic fish in spiral motion.

The spiral motion was the result of a combination of non-zero Δd and non-zero oscillating offset ξ_1 of the tail. A_1 and f_1 of the tail are 20° and 3.0 Hz, respectively. As shown

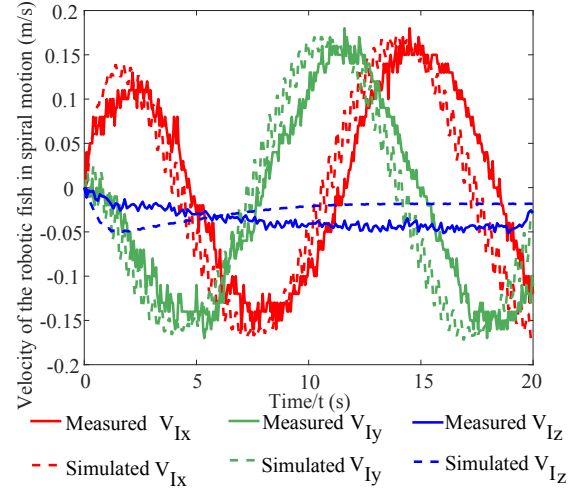


Fig. 18. Real-time velocity of the robotic fish in spiral motion.

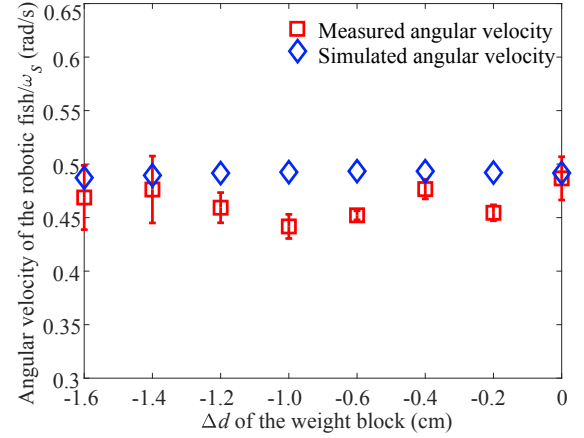


Fig. 19. Measured and simulated spiral angular velocity of the robotic fish.

in Figure 17, yaw angle of the robotic fish oscillates around varied values with the time, while pitch angle and the roll angle oscillate around constant values. It can be seen that the simulated attitudes closely track the measured attitudes. The velocity V_{I_x} along the axis $O_I X_I$ and the velocity V_{I_y} along the axis $O_I Y_I$ exhibit sine-like characteristics. The velocity V_{I_z} along the axis $O_I Z_I$ gradually researches a negative value, which means the robotic fish is spiralling up. Figure 19 and Figure 20 shows the measured and simulated spiral angular velocity ω_s and spiral velocity U_s of the robotic fish, respectively. It can be seen that both the ω_s and the U_s barely change with the Δd . The maximum and average percentage error of the ω_s are 3.6004% and 1.9323%, respectively. The maximum and average percentage error of the U_s are 11.4808% and 5.8953%, respectively. Figure 21 shows the measured and simulated spiral trajectory of the robotic fish in spiral motion. The measured trajectory tracks the simulated trajectory well with a maximum error of 0.3974 m.

V. CONCLUSION AND FUTURE WORK

In this article, a dynamic model that accounts for multiple three-dimensional motions, including rectilinear motion, turn-

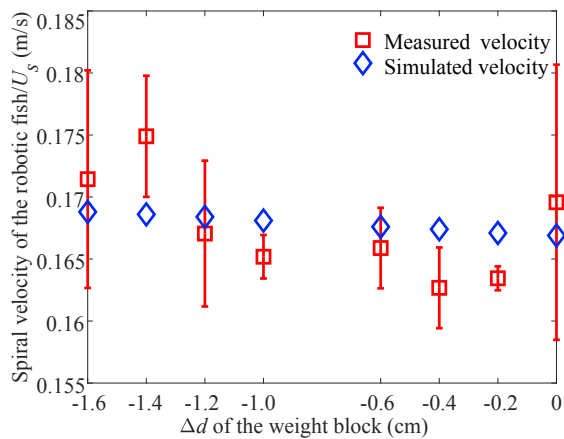


Fig. 20. Measured and simulated spiral velocity of the robotic fish.

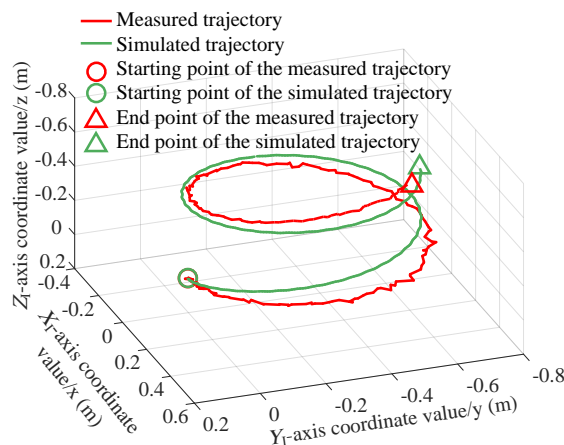


Fig. 21. Spiral trajectory of the robotic fish in spiral motion.

ing motion, gliding motion, and spiral motion, of an active-tail-actuated robotic fish with barycentre regulating mechanism was proposed basing on Newton-Euler method. CAD software SolidWorks, HyperFlow based computational fluid dynamics (CFD) simulation, and grey-box model estimation method are used for determining model parameters. Massive kinematic experiments with robotic fish prototype and numerical simulations demonstrate that the proposed model is capable of evaluating the trajectory, attitudes, and motion parameters including the linear velocity, motion radius, angular velocity, etc., for the robotic fish with small errors.

We are conducting researches on evaluating motion parameters of the robotic fish using its onboard ALLS, and an evaluation model that links the linear velocity, angular velocity, and motion radius to the hydrodynamic pressure variations (PVs) surrounding the fish body has been preliminarily acquired. Using the PVs measured by the ALLS, the above-mentioned motion parameters can be evaluated by solving the evaluation model inversely. In the future work, we will input the ALLS-evaluated motion parameters into a dynamic model-based controller as feedback terms, for adjusting the oscillation parameters of the robotic fish, and finally realizing flow-aided closed-loop control for the trajectory of the robotic fish.

ACKNOWLEDGMENT

This work was supported in part by grants from the National Natural Science Foundation of China (NSFC, No. 91648120, 61633002, 51575005) and the Beijing Natural Science Foundation (No. 4192026).

REFERENCES

- [1] R. Salazar, V. Fuentes, and A. Abdelkefi, "Classification of biological and bioinspired aquatic systems: A review," *Ocean Engineering*, vol. 148, pp. 75–114, Jan. 2018.
- [2] O. Khatib, X. Yeh, G. Brantner, B. Soe, B. Kim, S. Ganguly, H. Stuart, S. Wang, M. Cutkosky, A. Edsinger *et al.*, "Ocean one: A robotic avatar for oceanic discovery," *IEEE Robotics & Automation Magazine*, vol. 23, no. 4, pp. 20–29, Dec. 2016.
- [3] S. W. Huang, E. Chen, and J. Guo, "Efficient seafloor classification and submarine cable route design using an autonomous underwater vehicle," *IEEE Journal of Oceanic Engineering*, vol. 43, no. 1, pp. 7–18, Jan. 2018.
- [4] Y. S. Ryuh, G. H. Yang, J. Liu, and H. Hu, "A school of robotic fish for mariculture monitoring in the sea coast," *Journal of Bionic Engineering*, vol. 12, no. 1, pp. 37–46, Mar. 2015.
- [5] J. E. Chang, S. W. Huang, and J. H. Guo, "Hunting ghost fishing gear for fishery sustainability using autonomous underwater vehicles," in *Autonomous Underwater Vehicles (AUV)*, 2016 IEEE/OES, Nov. 2016, pp. 49–53.
- [6] Z. Wu, J. Liu, J. Yu, and H. Fang, "Development of a novel robotic dolphin and its application to water quality monitoring," *IEEE/ASME Transactions on Mechatronics*, vol. 22, no. 5, pp. 2130–2140, Oct. 2017.
- [7] A. Vasilijevic, D. Nad, F. Mandic, N. Miskovic, and Z. Vukic, "Coordinated navigation of surface and underwater marine robotic vehicles for ocean sampling and environmental monitoring," *IEEE/ASME Transactions on Mechatronics*, vol. 22, no. 3, pp. 1174–1184, Jun. 2017.
- [8] Y. Shi, C. Shen, H. Fang, and H. Li, "Advanced control in marine mechatronic systems: A survey," *IEEE/ASME Transactions on Mechatronics*, vol. 22, no. 3, pp. 1121–1131, Jun. 2017.
- [9] H. Li and W. Yan, "Model predictive stabilization of constrained underactuated autonomous underwater vehicles with guaranteed feasibility and stability," *IEEE/ASME Transactions on Mechatronics*, vol. 22, no. 3, pp. 1185–1194, Jun. 2017.
- [10] Y. Han, B. Wang, Z. Deng, and M. Fu, "A matching algorithm based on the nonlinear filter and similarity transformation for gravity-aided underwater navigation," *IEEE/ASME Transactions on Mechatronics*, vol. 23, no. 2, pp. 646–654, Apr. 2018.
- [11] —, "A combined matching algorithm for underwater gravity-aided navigation," *IEEE/ASME Transactions on Mechatronics*, vol. 23, no. 1, pp. 233–241, Feb. 2018.
- [12] X. Zheng, C. Wang, R. Fan, and G. Xie, "Artificial lateral line based local sensing between two adjacent robotic fish," *Bioinspiration & biomimetics*, vol. 13, no. 1, p. 016002, Nov. 2017.
- [13] A. Aggarwal, P. Kampmann, J. Lemburg, and F. Kirchner, "Haptic object recognition in underwater and deep-sea environments," *Journal of field robotics*, vol. 32, no. 1, pp. 167–185, Jan. 2015.
- [14] W. Wang, J. Liu, G. Xie, L. Wen, and J. Zhang, "A bio-inspired electrocommunication system for small underwater robots," *Bioinspiration & biomimetics*, vol. 12, no. 3, p. 036002, Mar. 2017.
- [15] E. R. Marques, J. Pinto, S. Kragelund, P. S. Dias, L. Madureira, A. Sousa, M. Correia, H. Ferreira, R. Gonçalves, R. Martins *et al.*, "Auv control and communication using underwater acoustic networks," in *OCEANS 2007-Europe*, Jun. 2007, pp. 1–6.
- [16] C. Shen, B. Buckham, and Y. Shi, "Modified c/gmres algorithm for fast nonlinear model predictive tracking control of auvs," *IEEE Transactions on Control Systems Technology*, vol. 25, no. 5, pp. 1896–1904, Sept. 2017.
- [17] C. Shen, Y. Shi, and B. Buckham, "Path-following control of an auv: A multiobjective model predictive control approach," *IEEE Transactions on Control Systems Technology*, vol. PP, no. 99, pp. 1–9, Jan. 2018.
- [18] —, "Trajectory tracking control of an autonomous underwater vehicle using lyapunov-based model predictive control," *IEEE Transactions on Industrial Electronics*, vol. 65, no. 7, pp. 5796–5805, Jul. 2018.
- [19] J. Yu, L. Liu, and M. Tan, "Three-dimensional dynamic modelling of robotic fish: simulations and experiments," *Transactions of the Institute of Measurement and Control*, vol. 30, no. 3–4, pp. 239–258, Aug. 2008.

- [20] J. Yu, M. Wang, Z. Su, M. Tan, and J. Zhang, "Dynamic modeling of a cpg-governed multi-joint robotic fish," *Advanced Robotics*, vol. 27, no. 4, pp. 275–285, Feb. 2013.
- [21] S. Zhang, J. Yu, A. Zhang, and F. Zhang, "Spiraling motion of underwater gliders: Modeling, analysis, and experimental results," *Ocean Engineering*, vol. 60, no. 3, pp. 1–13, Jan. 2013.
- [22] Z. Chen, J. Yu, A. Zhang, and F. Zhang, "Design and analysis of folding propulsion mechanism for hybrid-driven underwater gliders," *Ocean Engineering*, vol. 119, pp. 125–134, May. 2016.
- [23] Z. Chen, S. Shatara, and X. Tan, "Modeling of biomimetic robotic fish propelled by an ionic polymer–metal composite caudal fin," *IEEE/ASME Transactions on Mechatronics*, vol. 15, no. 3, pp. 448–459, Jun. 2010.
- [24] J. Wang and X. Tan, "A dynamic model for tail-actuated robotic fish with drag coefficient adaptation," *Mechatronics*, vol. 23, no. 6, pp. 659–668, Aug. 2013.
- [25] —, "Averaging tail-actuated robotic fish dynamics through force and moment scaling," *IEEE Transactions on Robotics*, vol. 31, no. 4, pp. 906–917, Aug. 2015.
- [26] F. Zhang, F. Zhang, and X. Tan, "Tail-enabled spiraling maneuver for gliding robotic fish," *Journal of Dynamic Systems, Measurement, and Control*, vol. 136, no. 4, p. 041028, May. 2014.
- [27] F. Zhang, J. Thon, C. Thon, and X. Tan, "Miniature underwater glider: Design and experimental results," *IEEE/ASME Transactions on Mechatronics*, vol. 19, no. 1, pp. 394–399, Feb. 2014.
- [28] G. Ozmen Koca, C. Bal, D. Korkmaz, M. C. Bingol, M. Ay, Z. H. Akpolat, and S. Yetkin, "Three-dimensional modeling of a robotic fish based on real carp locomotion," *Applied Sciences*, vol. 8, no. 2, p. 180, Jan. 2018.
- [29] J. L. Tangorra, C. J. Esposito, and G. V. Lauder, "Biorobotic fins for investigations of fish locomotion," in *2009 IEEE/RSJ International Conference on Intelligent Robots and Systems*. IEEE, 2009, pp. 2120–2125.
- [30] D. Yun, S. Kim, K.-S. Kim, J. Kyung, and S. Lee, "A novel actuation for a robotic fish using a flexible joint," *International Journal of Control, Automation and Systems*, vol. 12, no. 4, pp. 878–885, 2014.
- [31] K. A. Morgansen, B. I. Triplett, and D. J. Klein, "Geometric methods for modeling and control of free-swimming fin-actuated underwater vehicles," *IEEE Transactions on Robotics*, vol. 23, no. 6, pp. 1184–1199, Dec. 2007.
- [32] S. Chen, J. Wang, and X. Tan, "Target-tracking control design for a robotic fish with caudal fin," in *Proceedings of the 32nd Chinese Control Conference*. IEEE, 2013, pp. 844–849.
- [33] Y. Hu, W. Zhao, and L. Wang, "Vision-based target tracking and collision avoidance for two autonomous robotic fish," *IEEE Transactions on Industrial Electronics*, vol. 56, no. 5, pp. 1401–1410, 2009.
- [34] E. Krause, *Fluid Mechanics: With Problems and Solutions, and an Aerodynamics Laboratory*. Springer, 2005.
- [35] X. He, X. He, L. He, Z. Zhao, and L. Zhang, "Hyperflow: A structured/unstructured hybrid integrated computational environment for multi-purpose fluid simulation," *Procedia Engineering*, vol. 126, pp. 645–649, Dec. 2015.
- [36] X. He, L. Zhang, Z. Zhao *et al.*, "Validation of hyperflow in subsonic and transonic flow," *Acta Aerodynamica Sinica*, vol. 34, no. 2, pp. 267–275, Apr. 2016.
- [37] L. Ljung, *System identification toolbox: User's guide*. Citeseer, 1995.



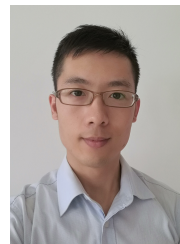
Minglei Xiong received the B.E. in North China Electric Power University (NCEPU), Beijing, China in 2012. He is currently a PhD candidate in General Mechanics and Foundation of Mechanics at Peking University. His current research interests include biomimetic robotics, artificial intelligent, and game theory.



Junzheng Zheng received the B.E. in Mechanical Design, Manufacturing and Automation from Huazhong University of Science and Technology, Wuhan, China in 2017. He is currently pursuing a master's degree in Control Theory and Control Engineering at Peking University. His current research interests include biomimetic robotics and lateral line inspired sensing.



Manyi Wang received the B.E. in Measurement and Control Technology and Instrumentation from National University of Defense Technology, Changsha, China in 2009. He is currently pursuing a master's degree in Control Theory and Control Engineering at Peking University. His current research interests include biomimetic robotics and lateral line inspired sensing.



Runyu Tian received the B.E. in Aircraft System and Engineering from National University of Defense Technology, Changsha, China in 2011. He is currently pursuing a master's degree in Control Theory and Control Engineering at Peking University. His current research interests include computational fluid dynamics, biomimetic robotics, and deep reinforcement learning.



Guangming Xie received his B.S. degrees in both Applied Mathematics and Electronic and Computer Technology, his M.E. degree in Control Theory and Control Engineering, and his Ph.D. degree in Control Theory and Control Engineering from Tsinghua University, Beijing, China in 1996, 1998, and 2001, respectively. Then he worked as a postdoctoral research fellow in the Center for Systems and Control, Department of Mechanics and Engineering Science, Peking University, Beijing, China from July 2001 to June 2003. In July 2003, he joined the Center as a

lecturer. Now he is a Full Professor of Dynamics and Control in the College of Engineering, Peking University.

He is an Associate Editor of Scientific Reports, International Journal of Advanced Robotic Systems, Mathematical Problems in Engineering and an Editorial Board Member of Journal of Information and Systems Science. His research interests include smart swarm theory, multi-agent systems, multi-robot cooperation, biomimetic robot, switched and hybrid systems, and networked control systems.



Xingwen Zheng received the B.E. in Mechanical Engineering and Automation from Northeastern University, Shenyang, China in 2015. He is currently a PhD candidate at the Intelligent Biomimetic Design Lab, State Key Laboratory for Turbulence and Complex Systems, College of Engineering, Peking University, Beijing, China. His current research interests include biomimetic robotics, lateral line inspired sensing, and multi-robot control.